RSC Advances

ROYAL SOCIETY OF CHEMISTRY

www.rsc.org/advances

Journal Name

ARTICLE

Inorganic dye-sensitized solar cell employing In-enriched Cu-In-S ternary colloids prepared in water media

S. Higashimoto,[a]* S. Inui,[a] T. Nakase,[a] M. Azuma,[a] M. Yamamoto[b] and M. Takahashi[b]

Received 00th January 20xx,

Accepted 00th January 20xx

DOI: 10.1039/x0xx00000x

www.rsc.org/

Copper-indium-sulfer (CIS) ternary colloids with different chemical compositions (In/Cu = 1, 2, 3 and 4) were synthesized in "green" water media at 298 K. It was observed that these CIS colloidal particles possess identical crystal structures in tetrahedron. They exhibit energy gaps at 1.7 ~ 2.0 eV, which is attributed to the quantum size effects through a decrease of particle sizes from 4 to 2 nm. It was also found that the photoelectrodes employing CIS colloids with the In-enriched compositions exhibit high incident photon to current efficiency (IPCE) up to ca. 780 nm. The solar cell constructed by CIS-TiO_2||S_x^{2-}/xS^{2-}||carbon electrode exhibited a power conversion efficiency (PCE) up to ca. 2.5%. Furthermore, the CIS-TiO_2 photoelectrode coated with ZnS as passivation layers by SILAR processes exhibited a remarkable improvement of the PCE up to 3.54% (short-circuit current: 8.72 mA/cm^2, open-circuit voltage: 750 mV and fill factor: 53.6%). Effects of chemical compositions and ZnS coating to the photoelectrodes were further discussed by electrochemical impedance spectroscopy.

Introduction

Semiconductor nanoparticles are one of the most promising photo-functional materials for such applications as solar cells, light emitting diodes and fluorescence.[1] In particular, the quantum dot sensitized solar cells (QDSC) are considerably paid attention since the theoretical power conversion efficiencies (PCE) of these cells have potentials to surpass the Shockley-Queisser limit (31%).[2] It was reported that the PCE on the PbS QDSC exhibited over 7%.[3] However, such quantum dots as CdSe, CdS, CdTe, PbS, PbSe have a drawback of containing highly toxic components that severely restricts their possible applications.[4-6]

One of the promising materials is copper indium sulfide ($CuInS_2$, CIS) which involves less toxic elements. They have characteristic features as follows: the absorption spectra are tunable by changing particle sizes (~ 5 nm), and an extinction coefficient of ~ 10^5 cm^{-1} (at 500 nm) of which the value is ca. 10 times higher than that for CdTe or N719 (organic dyes) for dye-sensitized solar cells (DSSC).[7, 8] Recently, solution-processed CIS QDSC can be expected to offer a cost reduction for fabrication and high efficiency.[9-22] In general, the CIS colloids were prepared in organic solvents using such long fat chain as 1-dodecanethiol involving oleylamine (capping agents) at relatively high temperature (373 ~ 473 K). Further, recapping with such short ligands as 3-mercaptopropionic acid (MPA) was carried out in order to achieve strong interaction of CIS colloids with TiO_2 surface.[9-16] Among them, the CIS/ZnS (QDSC)-TiO_2 photoelectrode was found to exhibit the highest PCE yielding with 7.04%.[16]

Water is considered to be environment-friendly solvent and provides simple synthetic routes of CIS colloids without ligand-exchanging.[17-22] However, the photoelectrodes employing CIS colloids prepared in water relatively exhibit low solar cell performance, yielding with at most 2.52% even in the Cu_2S/CIS/ZnSe cascade-type electronic structures.[20] Along these backgrounds, our purpose is to design CIS colloids prepared in water, and to develop the QDSC performances in the absence of toxic compounds involving Cd, Pb and Se etc.

Development of counter electrodes is also important factors for an improvement of the solar cell performance. Recently, the porous Cu_2S, Cu_2S-RGO and Pt were used as counter electrodes for $CuInS_2$ QDSC.[8-22] On the other hand, carbons are one of the promising materials, which are electrically conductive and show catalytic activity for the reduction of triiodide.[23-28] Therefore, carbon electrodes employing carbon nanotube, mesoporous carbon and carbon black have been extensively studied for the dye-sensitized solar cell (DSSC). However, the utilization of carbon-based electrodes is few reported for the CIS QDSC.

In this study, we have investigated synthesis of the CIS colloidal particles with different chemical compositions (In/Cu = 1, 2, 3 and 4) in water at 298 K, characterizations and their application to the inorganic dye-sensitized solar cell. In particular, the relationship between optical properties of CIS colloids and solar cell performances has been studied.

Experimental

Preparation of Cu-In-S ternary colloids

The Cu-In-S ternary (CIS) colloids with different chemical compositions of In/Cu were prepared according to the previous literature with partial modification.[17] 0.125 M aq. $Cu(OAc)_2$ (2 mL)

[a] College of Engineering, Osaka Institute of Technology, 5-16-1 Omiya, Asahi-ku, Osaka 535-8585, Japan.
[b] Osaka Municipal Technical Research Institute, 1-6-50 Morinomiya, Joto-ku, Osaka 536-0025, Japan.

Electronic Supplementary Information (ESI) available: Characterizations of electrodes by XRD, XPS, SEM (EDX), CV and EIS data. See DOI: 10.1039/x0xx00000x

and 0.125 M aq. $InCl_3$ (2, 4, 6 and 8 mL) were added into de-aerated distilled water (140 mL) under N_2 bubbling for 30 min at 298 K. When 2.35 M aq. thioglycolic acid (TGA, 1 mL) as a capping agent was added into the solution, it became simultaneously black and then it gradually turned colorless. Subsequently, 0.5 M aq. Na_2S (1 mL) was introduced quickly to form colloids in orange to brown. The colloidal solutions were concentrated by rotary evaporator and the volume was adjusted to 50 mL.

Characterizations of CIS colloids

UV-Vis spectra of CIS colloids were obtained in a transmittance mode using a UV-Vis spectrophotometer (UV-3100PC, Shimadzu). The colloidal solutions were diluted by 10 times with water prior to measurements.

X-ray diffraction (XRD) patterns were obtained with a RIGAKU RINT2000 diffractometer using Cu K_α radiation (λ = 1.5417 Å). In order to evaluate XRD patterns of the CIS, the colloidal solutions were precipitated by adding ethanol as poor solvents. Solid products were collected by centrifuge and dried. It should be noted that the solid products can be re-dispersed in water.

DLS (Dynamic Light Scattering) was used to characterize size of colloidal particles as prepared by particle size analyzer (ELSZ series, Ohtsuka Co. Ltd.).

Preparation of CIS-TiO_2 thin films

TiO_2 powder (2.85 g of Degussa P-25 and 0.15 g of ST-01) was added into dil. HNO_3 (5 mL, pH 3) involving polyethyleneglycol (H_w = 20000, 0.3 g) and Toriton X-405 (0.3 mL), and they were dispersed by a supersonification. The paste was then spread onto an ITO-glass electrode (10 Ω/cm^2, Geomatec) by spin coating (3000 rpm, 3 min), followed by heat-treatment at 673 K for 1 h in air. This process was repeated twice, and thickness of the TiO_2 film was adjusted to be ca. 15 μm.

The TiO_2 film was immersed in the solution involving CIS colloids at 313 K for 20 h, and then washed with acetonitrile in order to remove weakly adsorbed colloids. Furthermore, the photoelectrodes were coated with ZnS by successive ionic layer adsorption and reaction (SILAR) process. The CIS-TiO_2 photoelectrodes were immersed into 0.1 M aq. $Zn(NO_3)_2$ for 60 s, and 0.1 M aq. Na_2S for 60 s by turn at 298 K. Before each immersion, the photoelectrode was rinsed with acetonitrile and dried under air.

Characterization of CIS-TiO_2 thin films

The morphology of films was characterized by field emission scanning electron microscope (FE-SEM, JEOL JSM-840A). The chemical compositions of Cu, In and S adsorbed on the TiO_2 were determined by energy dispersive X-ray (EDX) spectroscopy (JSM-6610, JEOL) and the results are shown in Table 1. For example, the ZnS(6)/CIS123-TiO_2 represents for the CIS colloids in the ratio of Cu : In : S (= 1 : 2 : 3) anchored on TiO_2, and ZnS coating with 6 cycles by SILAR process.

Further, XPS analysis indicates that CIS123-TiO_2 involves Cu^+, In^{3+} and S^{2-} ions (See Fig. SI 1). This result indicates that the TGA can reduce Cu^{2+} into Cu^+ ions during the preparation of CIS colloids at 298 K.[29]

Table 1 Chemical compositions of several CIS-TiO_2 photoelectrodes determined by EDX analysis.

Ratio of In/Cu	Chemical compositions			photoelectrodes
	Cu	In	S	
1	1.00	0.95	2.08	CIS112-TiO_2
2	1.00	1.91	3.36	CIS123-TiO_2
3	1.00	3.35	5.65	CIS135-TiO_2
4	1.00	3.86	6.95	CIS147-TiO_2

Preparation of carbon electrode

The TiO_2 colloid was prepared in accordance with previous report:[28] titanium isopropoxide (12.5 mL) with isopropanol (2 mL) was added dropwise to water (75 mL) under stirring. After an addition of 65% nitric acid (0.6 mL), the solution was heated at 80°C for 8 h under stirring. As a result, the TiO_2 precipitate was peptized to a white semi-transparent colloid. Carbon black powder (100 mg, 1270 m^2/g, Ketchen black, KB600, Lion Corp.) was ground in a mortar with 0.1 mL of TiO_2 colloid for an increase of surface area, carbon black (1.0 g, Tokai Carbon Co., Ltd.) and distilled water (1-2 mL). The carbon paste was spread on graphite plate (5×5 mm, Nilaco) by spin-coating (3000 rpm, 2 min). The substrate was heated in air at 573 K for 10 min to fabricate modified-carbon electrode.

Photo-electrochemical measurements

Photo-electrochemical measurements were performed with no bias in a two-electrode system constructed by the CIS-TiO_2||polysulfide (S_x^{2-}/xS^{2-})||carbon electrode. The polysulfide electrolyte consists of 1.0 M Na_2S and 10 mM S in 0.5 M aq. Na_2SO_4. The distance between two electrodes was adjusted to ca. 2 mm.

J-V curves were recorded by a Potentiostat/Galvanostat (HABF5001, HOKUTO DENKO) under global AM 1.5 solar irradiation (100 mA/cm^2) using a simulator (XES-40S1, SAN-EI Electric Co. Ltd.) calibrated with a Si-based reference (BS-520BK, Bunkoukeiki Co., Ltd.). The photovoltaic parameters such as short-circuit photocurrent (J_{sc}), open-circuit voltage (V_{oc}), fill-factor (*FF*) and power conversion efficiencies (PCE) were extracted from *J-V* curves.

In order to identify incident photon-to-current efficiencies (IPCE), photocurrents were measured with no bias under monochromatic irradiation through several band-path filters from 100 W xenon lamp (LAX CUTE, Asahi Spectra Co. Ltd.). The photon energy was adjusted to an energy flux of 0.1 - 0.2 mW/cm^2 by the power meter (ORION/PD, Ophir). The IPCE for each photoelectrode was calculated by an equation (1):

$$IPCE\ (\%) = (124 \times J_{ph}) / (\lambda \times P_{in}) \quad (1)$$

, where J_{ph} is the photocurrent (μA/cm^2), λ is the wavelength (nm) of the incidental photon, and P_{in} is the power of the incident light (mW/cm^2).

Electrochemical impedance spectroscopy (EIS) was carried out using Potentio/Galvanostat (PGSTAT204, Autolab) with FRA analyzer in the frequency ranging from 10^{-1} to 10^5 Hz with a perturbation of 10 mV at open circuit voltage under global AM 1.5 solar irradiation (100 mA/cm^2).

Results and Discussion

Physico-chemical properties of CIS colloids

CIS colloids (In/Cu = 1, 2, 3 and 4) were prepared using TGA in water 298 K. The CIS colloid (In/Cu = 1) was likely to be aggregated within one week, probably due to the presence of many defect sites (dangling bonds).[9] On the other hand, the colloids (In/Cu = 2, 3 and 4) were stable at least for one month. Therefore, the CIS colloids can be stabilized by excess In^{3+} ions, probably leading to the reduction of defect sites. Furthermore, from the analysis of DLS, particle sizes of the CIS colloidal particles (In/Cu = 1, 2, 3 and 4) were determined to be 2.4 ± 0.6 nm, 2.9 ± 0.8 nm, 2.0 ± 0.4 nm and 1.7 ± 0.4 nm, respectively. These CIS colloids (In/Cu = 1 ~ 4) exhibit identical XRD patterns attributed to the tetragonal crystal structures, which are independent on the chemical compositions of In/Cu. Details are shown in Fig. SI 2.

UV-Vis absorption spectra of CIS colloids (In/Cu = 1, 2, 3 and 4) as prepared are shown in Fig. 1. The CIS colloids exhibits energy gaps in the range of 1.7 ~ 2.0 eV, which is wider than that of the bulk $CuInS_2$ (1.5 eV).[7] The absence of sharp excitonic features in the absorption spectra is due to the heterogeneous nano-colloids with different sizes. The absorption in visible-light region is mainly attributed to the electronic transition from the hybrid orbitals of Cu 3d + S 3p to In 5s5p.[30] It was also observed that the optical absorption of the In-enriched CIS colloids (In/Cu = 2, 3 and 4) is larger than that of the CIS colloid (In/Cu = 1). In order to clarify the effects of chemical compositions on the optical properties, the differential spectra of CIS colloids were shown in inset of Fig. 1. It was observed that the ΔA at the wavelengths shorter than 800 nm increased in the differential absorption spectra between CIS112-TiO_2 and CIS123-TiO_2, while that shorter than 680 nm increased in the differential spectra between CIS112-TiO_2 and CIS147-TiO_2. The energy gaps of CIS colloids were observed to increase with increasing of the ratio of In/Cu. That is, chemical compositions of CIS colloids significantly change the optical properties. Moreover, the energy gaps of CIS colloids were confirmed to increase with decreasing of particle sizes due to the quantum confinement. (See relationship between particle sizes of CIS colloids and energy gaps in Fig. SI 3.)

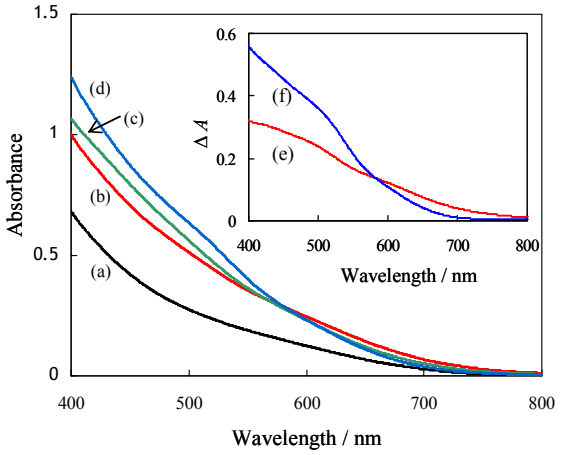

Fig. 1 UV-Vis spectra of CIS colloids: In/Cu = 1 (a), 2 (b), 3 (c) and 4 (d). Differential spectra (inset) of (b) - (a): (e); and (d) - (a): (f).

When the TiO_2 films are immersed in the CIS colloidal solutions, the CIS colloidal particles are strongly adsorbed on the TiO_2 by the electrostatic interaction between negatively-charged CIS colloids by the carboxylate anions and positively-charged titanium cations.[31, 32] Figure 2 shows SEM and TEM images of the TiO_2 films before and after immersing CIS colloids. It was observed that the TiO_2 particles were observed to be large by adsorption of CIS colloids. Each CIS-TiO_2 particle formed good inter-connection between particles can be expected to improve the electrical contact and conductivity of thin films which enhance charge-carrier transfer properties. The particle sizes of TiO_2 and CIS123-TiO_2 were measured to be 35±10 and 50±10 nm, respectively (See Fig. SI 4). From EDX spectroscopic measurements, Cu, In and S elements are homogeneously distributed in the cross-sections of the CIS123-TiO_2 (see Fig. SI 5). It should be noted that the particle size of the CIS112-TiO_2, CIS135-TiO_2 and CIS147-TiO_2 is larger than that of bare TiO_2, and ZnS coating on the CIS123-TiO_2 surface prevents the block of nano-channels (See Fig. SI 6). Characteristic XRD patterns attributed to the CIS particles in several CIS-TiO_2 and ZnS/CIS-TiO_2 electrodes were not clearly detected (See Fig. SI 7), suggesting that the CIS particles are highly dispersed on the TiO_2. Moreover, the ZnS on ZnS(6)/CIS123-TiO_2 was found to form an amorphous structure. On the other hand, UV-Vis spectra of the CIS-TiO_2 and ZnS-coated CIS-TiO_2 exhibit visible-light absorption (See Fig. SI 8). It is noted that the absorption edge of the CIS-TiO_2 are almost identical with those of corresponding CIS colloidal particles (Compare Fig. SI 8 [I] with Fig. 1). Moreover, ZnS/CIS-TiO_2 did not significantly change the absorption edge even when the number of SILAR cycles increase (See Fig. SI 8 [II]).

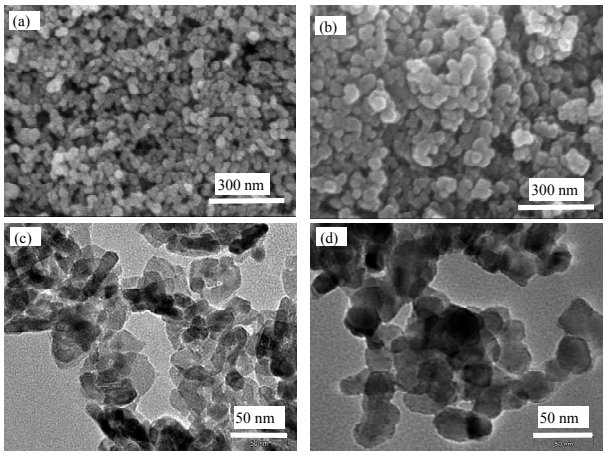

Fig. 2 SEM (a, b) and TEM images (c, d) for TiO_2 (a, c) and CIS123-TiO_2 (b, d).

Solar cell performances of CIS-TiO_2 photoelectrodes

In order to understand the photo-response center, IPCE was measured with no bias under monochromatic irradiation in a two-electrode system of CIS-TiO_2||(S_x^{2-}/xS^{2-})||carbon electrode as shown in Fig. 3 [I]. The solar cell employing CIS112-TiO_2 exhibits IPCE of 0.52% at 710 nm, 6.2% at 600 nm and 18.2% at 510 nm. Moreover, the CIS-TiO_2 with In-enriched compositions (In/Cu = 2, 3 and 4) exhibited significant improvement of IPCE. The differential plots of IPCE derived CIS112-TiO_2 from CIS123-TiO_2 shows a remarkable improvement of the photo-response at shorter

wavelengths than 780 nm (e) and those derived CIS112-TiO_2 from CIS147-TiO_2 at shorter wavelengths than 680 nm (f) as shown in Fig. 3 [II]. Compared with UV-Vis spectra shown in Fig. 1, the photo-action spectra of the IPCE can correspond with photo-absorption, which are influenced by the CIS particle sizes.

The *J-V* curves of solar cells constructed by CIS-TiO_2||(S_x^{2-}/xS^{2-})||carbon electrode are shown in Fig. 4, and photovoltaic parameters are shown in Table 2. When the graphite electrode without surface modification was used, the solar cell employing CIS112-TiO_2 exhibited low PCE yielding with only 0.22%. On the other hand, when the graphite electrode modified with porous carbons were used, the solar cell employing CIS112-TiO_2 exhibits 2.85 mA/cm^2 for J_{SC}, 0.68 V for V_{OC} and 44.7% for *FF*, yielding with the PCE of 0.87%. Therefore, the surface modification of graphite electrode with porous carbon plays a significant role in an improvement of the catalytic reduction of polysulfide ions (See Figs. SI 9 and 10).[33]

Furthermore, it was observed that CIS123-TiO_2, CIS135-TiO_2 and CIS147-TiO_2 exhibit 300, 320 and 280% increase of PCE compared with CIS112-TiO_2, respectively. In particular, photocurrents were significantly increased on the photoelectrodes employing In-enriched CIS colloids. In order to improve the photovoltaic performance, the SILAR process for coating with ZnS was subsequently employed. When the number of SILAR cycles was increased to six, the best photovoltaic performance was obtained, i.e., short-circuit current: 8.72 mA/cm^2, open-circuit voltage: 750 mV, fill factor: 53.6% and PCE: 3.54%. This value is the highest among the solar cells employing CIS colloids prepared in water media. It was also observed that the solar cells exhibited good re-producibilities for the PCE (See Fig. SI 11). Furthermore, the photo-stability of solar cells was evaluated. The PCE was observed to decrease to ca. 20% on the CIS123-TiO_2 after consecutive photo-irradiation for 2 h, while to ca. 65% on the ZnS(6)/CIS123-TiO_2 (See Fig. SI 12). The CIS-TiO_2 photoelectrode was thus confirmed to exhibit good photo-stability by ZnS coating.

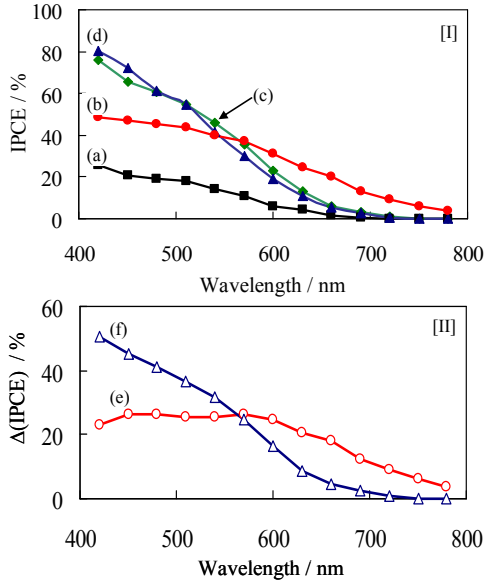

Fig. 3 IPCE for [I] CIS112-TiO_2 (a), CIS123-TiO_2 (b), CIS135-TiO_2, (c) CIS147-TiO_2 (d); and [II] the differential IPCE (Δ IPCE) of (b) - (a): (e); and (d) - (a): (f).

To gain further insight into the electron transport and recombination properties, the EIS was applied for several CIS-TiO_2 photoelectrodes. Figure 5 (a) shows Nyquist plots for the solar cell employing a CIS123-TiO_2 photoelectrode. It is composed of a semicircle at high frequencies and a straight line at low frequencies, which correspond with an equivalent circuit of a charge-transfer impedance (R_{CT}) at the TiO_2/CIS interface and diffused impedance (Warburg impedance, Z_W) at the CIS/electrolyte interfaces, respectively (See inset of Fig. 5).[14] It was also observed that Ohmic impedance (R_S) for all the cells were identical to be ca. 17 Ω, while the impedance at the counter electrode/electrolyte interfaces is too small to be evaluated. Table 2 also shows R_{CT} parameters of several CIS-TiO_2 photoelectrodes having different ratios of In/Cu. It was observed that the R_{CT} is likely to decrease with increasing the ratio of In/Cu. This is probably due to the reduction of trapping defect sites by the charge compensation with In^{3+} ions. Moreover, the R_{CT} of the ZnS(6)/CIS123-TiO_2 dramatically decreased from 34 to 13 Ω/cm^2 as shown in Fig. 5 (b). It was, thus, found that the lower the R_{CT} are, the higher solar cell performance becomes.

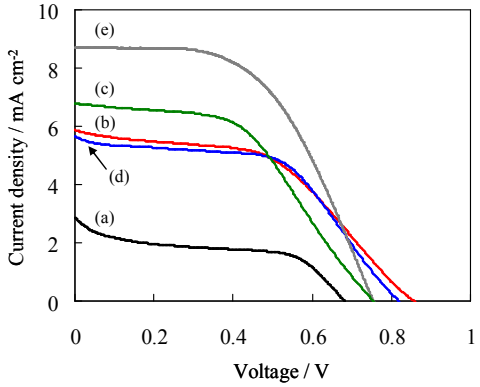

Fig. 4 *J-V* curves for the CIS112-TiO_2 (a), CIS123-TiO_2 (b), CIS135-TiO_2 (c) and CIS147-TiO_2 (d), and ZnS(6)/CIS123-TiO_2 (e). Counter electrode was employed with graphite carbon modified with porous carbon.

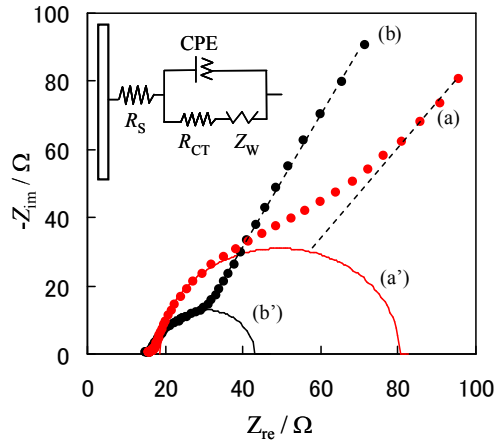

Fig. 5 Nyquist plots for the CIS123-TiO_2 (a, a') and ZnS(6)/CIS123-TiO_2 (b, b'), and their corresponding semicircles (a' - c'). The inset shows the equivalent circuit model: resistance of the electrolyte (R_s), charge transfer resistance (R_{ct}), Warburg resistance (Z_w) constant phase element (*CPE*).

Table 2 Photovoltaic and EIS parameters for several CIS-TiO_2 photoelectrodes using carbon electrode with carbon modification.

photoelectrodes	J_{SC} (mA/cm^2)	V_{OC} (V)	*FF* (%)	η (%)	[1)] R_{CT} (Ω)
[2)]CIS112-TiO_2	1.62	0.32	41.8	0.22	-
CIS112-TiO_2	2.85	0.68	44.7	0.87	45
CIS123-TiO_2	5.87	0.86	48.6	2.45	34
CIS135-TiO_2	6.78	0.75	49.4	2.53	25
CIS147-TiO_2	5.64	0.82	54.3	2.51	28
ZnS(6)/CIS123-TiO_2	8.72	0.75	53.6	3.54	13

1) Details are shown in Fig. SI 13. 2) Using graphic carbon without further modification as counter electrode.

In order to understand effects of the ZnS coating, the potentials for photo-charging and self-discharging in dark on the CIS123-TiO_2 and ZnS(6)/CIS123-TiO_2 were investigated, and the results are shown in Fig. 6. It was observed that the photo-charged potentials for the CIS123-TiO_2 and ZnS(6)/CIS123-TiO_2 electrodes reached at ca. -0.7 and -0.8 V vs. Ag/AgCl, respectively, under illumination with solar light. The photo-induced electrons are accumulated at the conduction band and/or surface states, while the ZnS coating does not significantly change the photo-charged potentials. Subsequently, self-discharging is induced by the internal chemical reactions between the photoelectrode and electrolyte. From these results, the ZnS coating as passivation layers retard the electron recombination at the TiO_2/electrolyte interface, leading to long lifetimes of the photo-induced electrons. The ZnS layers were, thus, confirmed to participate in an improvement of the solar cell performances.

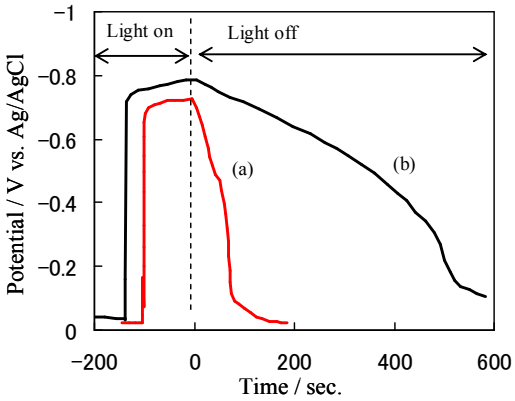

Fig. 6 Photo-charging and self-discharging for the solar cells employing CIS123-TiO_2 (a) and ZnS(6)/CIS112-TiO_2 (b).

Figure 7 shows photovoltaic mechanisms for ZnS/CIS-TiO_2||(S_x^{2-}/xS^{2-})||carbon electrode. The CIS sensitizer exhibits efficient charge separation to form electrons and holes under solar irradiation. In particular, ZnS with a wider band gap provides passivation effects for the leakage of electrons from the photoelectrodes to the electrolyte. Subsequently, the photo-induced holes in the CIS are scavenged by sulfide (S^{2-}) electrolytes, while electrons are injected into the TiO_2 conduction band, followed by reduction of polysulfide ions (S_x^{2-}) at the carbon electrode. It should be noted that the V_{OC} corresponds with the difference between redox potentials of S^{2-}/S_x^{2-} and the Fermi levels of CIS/TiO_2 photoelectrodes.

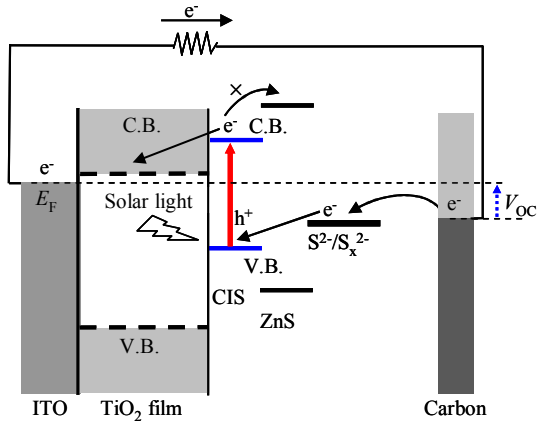

Fig. 7 photovoltaic mechanisms for ZnS/CIS-TiO_2||(S_x^{2-}/xS^{2})||carbon electrode under solar-light illumination.

Conclusions

The Cu-In-S ternary colloids with different In/Cu compositions were prepared in "green" water media using thioglycolic acid as a capping agent at 298 K. These colloids were applied to the inorganic dye-sensitized solar cells, i.e., CIS-TiO_2||(S_x^{2-}/xS^{2-})||carbon electrode. As a consequence, they exhibited high PCE, yielding with 3.54% without such toxic elements as Cd and Pb. To our best knowledge, this value is the highest among the solar cells employing CIS colloids prepared in water media. High PCE is attributed to 1) the reduction of defect sites through the In-enriched CIS colloids, 2) the quantum confinement by a decrease in particle sizes, and 3) ZnS-passivation to suppress non-radiative recombination. Although CIS-TiO_2 photoelectrode employing CIS colloids prepared in water exhibit less efficient solar cell performance than that is previously prepared in organic solvent, the optimizations of capping agent, ZnS coating and counter electrode can be expected to improve the PCE. Our findings, thus, can contribute to design environment-friendly CIS-based solar cell.

Acknowledgements

This work was supported by JSPS KAKENHI Grant Number 26420730. We thank Profs. T. Kamegawa and M. Matsuoka at Osaka Prefecture University for their useful discussion with DLS and FE-SEM results.

Notes and references

1 S. Suresh, *Nanosci. Nanotechnol.*, 2013, **3**(3) 62.
2 W. Shockley, H. J. Queisser, *J. Appl. Phys.*, 1961, **32**, 510.
3 R. W. Crisp, D. M. Kroupa, A. R. Marshall, E. M. Miller, J. Zhang, M. C. Beard, J. M. Luther, *Sci. Rep.*, 2015, **5**, 9945.
4 P. V. Kamat, K. Tvrdy, D. R. Baker, J. G. Radich, *Chem. Rev.*, 2010, 110, 6664.
5 P. V. Kamat, *J. Phys. Chem. C*, 2007, **111**, 2834.
6 I. J. Kramer, E. H. Sargent, *Chem. Rev.*, 2014, **114**, 863.
7 B. Tell, J. Shay, H. Kasper, *Phys. Rev. B*, 1971, **4** (8) 2463.
8 M. Booth, A. P. Brown, S. D. Evans, K. Critchley, *Chem. Mater.*, 2012, **24**, 2064.
9 P. K. Santra, P. V. Nair, K. G. Thomas, P. V. Kamat, *J. Phys. Chem. Lett*., 2013, **4**, 722.
10 K-T Kuo, D-M Liu, S-Y Chen, C-C Lin, *J. Mater. Chem.*, 2009, **19**, 6780.
11 T-L Li, Y-L Lee, H. Teng, *J. Mater. Chem.*, 2011, **21**, 5089.
12 T-L Li, Y-L Lee, H. Teng, *Energy Environ. Sci*., 2012, **5**, 5315.
13 H. McDaniel, N. Fuke, N. S. Makarov, J. M. Pietryga, V. I. Klimov, *Nat. Commun.*, **2013**, 4, 2887.
14 C. C. Chang, J. K. Chen, C. P. Chen, C. H. Yang, J. Y. Chang, *ACS Appl. Mater. Interfaces*, 2013, **5**, 11296.
15 T-L Li, H. Teng, *J. Mater. Chem.*, 2010, **20**, 3656.
16 Z. Pan, I. Mora-Seró, Q. Shen, H. Zhang, Y. Li, J. Wang, X. Zhong, J. Bisquert, *J. Am. Chem. Soc.*, 2014, **136**, 9203.
17 X. Hu, Q. Zhang, X. Huang, D. Li, Y. Luo, Q. Meng, *J. Mater. Chem*., 2011, **21**, 15903.
18 Y. Wang, Y. Rui, Q. Zhang, Y. Li, H. Wang, *ACS Appl. Mater. Interfaces*, 2013, **5**, 11858.
19 X. Xu, Q. Wan, C. Luan, F. Mei, Q. Zhao, P. An, Z. Liang, G. Xu, J. A. Zapien, *ACS Appl. Mater. Interfaces*, 2013, **5**, 21, 10605.
20 J. Y. Chang, L-F Su, C-H Li, C-C Chang, J-M Lin, *Chem. Commun*., 2012,**48**, 4848.
21 Z. Peng, Y. Liu, W. Shu, K. Chen, W. Chen, *Chem. Phy. Lett*., 2013, **586**, 85.
22 J-J Wu, W-T Jiang, W-P Liao, *Chem. Commun*., 2010, **46**, 5885.
23 G. Li, F. Wang, Q. Jiang, X. Gao, P. Shen, *Angew. Chem., Int. Ed*., 2010, **49**, 3653.
24 S. I. Cha, B. K. Koo, S. H. Seo, D. Y. Lee, *J. Mater. Chem.,* 2010, **20**, 659.
25 B. Fang, S-Q Fan, J. H. Kim, M-S Kim, M. Kim, N. K. Chaudhari, J. Ko, J.-S. Yu, *Langmuir*, 2010, **26**, 11238.
26 J. Lim, S. Y. Ryu, J. Kim, Y. Jun, *Nanoscale Res. Lett.*, 2013, **8**(1), 227.
27 J. Chen, K. Li, Y. Luo, X. Guo, D. Li, M. Deng, S. Huang, Q. Meng, *Carbon*, 2009, **47**, 2704.
28 T. N. Murakami, S. Ito, Q. Wang, Md. K. Nazeeruddin, T. Bessho, I. Cesar, P. Liska, R. Humphry-Baker, P. Comte, P. Péchy, M. Grätzel, *J. Electrochem. Soc.,* 2006, **153**(12), A2255.
29 W. Yue, S. Han, R. Peng, W. Shen, H. Geng, F. Wu, S. Tao, M. Wang, *J. Mater. Chem.*, 2010, **20**, 7570.
30 I. Tsuji, H. Kato, H. Kobayashi, A. Kudo *J. Phys. Chem. B*, 2005, **109***,* 7323.
31 T. Ganesh, R.S. Mane, G. Cai, J. H. Chang, S. H. Han, *J. Phys. Chem. C*, 2009, **113**, 7666.
32 D. F. Watson, *J. Phys. Chem. Lett.*, 2010, **1**, 2299.
33 Surface morphology of the graphic electrode seems to be flat, while the surface modification with porous carbon exhibit high roughness. Graphite electrode exhibits cathodic currents by the catalytic reduction of S_x^{2-} ions. Furthermore, the cathodic current was significantly enhanced by the modification with porous carbon due to the high catalytic activities.